Competitive adsorption of water and chemical warfare agents on transition metal embedded graphene

Julien Claudot, Estelle Soubeyrand-Lenoir, Guillaume Maurin

Competitive adsorption of water and chemical warfare agents on transition metal embedded graphene

Julien Claudot [a], Estelle Soubeyrand-Lenoir[b], Guillaume Maurin[a*]

[a] ICGM, Univ. Montpellier, CNRS, ENSCM, Montpellier, France

[b] DGA Maîtrise NRBC, BP N°3-5 rue Lavoisier, 91710 Vert le Petit, France.

Abstract

Adsorption of three CWA molecules (soman, sarin and mustard gas) was systematically explored on transition metal (Chromium and Vanadium) embedded graphene models under dry and wet conditions. Density Functional Theory calculations first revealed that both metal@graphene substrates show a very high affinity for all CWAs under dry conditions, sarin being expected to be even more strongly coordinated since its associated adsorption energies above 43 kcal.mol^{-1} are higher than the values calculated for soman and mustard gas. Two different wet scenarios were further explored with the consideration of a pre-humidification and a simultaneous competitive adsorption of water with CWAs. These calculations evidenced that the presence of water decreases the CWA adsorption energy for sarin and soman in the two embedded graphene models by maximum 20%. Interestingly, we demonstrated that this decrease is much less pronounced (3.3%) in the case of gas mustard adsorbed on chromium embedded graphene. Such metal embedded carbon substrates are thus predicted to maintain globally high level of CWA capture performances under humidity which corresponds to the most common operating conditions of protective gas masks. An *In-depth* analysis of the interactions between the CWAs and the metal embedded graphene in the presence of water was further conducted to gain insight into the origin of this energetic trend at the electronic-level.

Keywords: Metal impregnated carbons; Chemical Warfare Agents; Water; Competitive Adsorption; Density functional theory.

1. Introduction

Chemical warfare agents (CWAs) are a major threat to human health owing to their potential usage as chemical weapons by terrorist groups. Sulfur mustard also known as mustard gas and nerve agents including sarin and soman are the most typical CWAs [1]. Sulfur mustard ($C_4H_8Cl_2S$), discovered accidentally in 1822 [2], is an alkylating agent capable of causing short and long term morbidity and was used during World War I [3]. The nerve agents are organophosphorus compounds containing P-X bonds (with X = Fluor in the case of sarin – $C_4H_{10}FO_2P$ and soman – $C_7H_{16}FO_2P$) discovered by Gerhard Schrader in 1937 [4] and they are among the deadliest CWAs to date. These nerve agents were used during World War II [5], as well as over the first Persian Gulf War [6, 7] and more recently in 1995 with the terrorist attacks in Tokyo [8, 9]. Despite the international ban on their uses [3], some of these CWAs are still considered as chemical weapons in modern warfare. Consequently, their detection and capture are still a vital concern. As a result, the use of porous materials, such as activated carbons owing to their large surface area and high chemical stability, has been envisaged as one of the most efficient strategies to adsorb CWAs [10-15]. However, the standard activated carbons suffer from a relatively poor affinity for polar molecules. This encouraged the community to take advantage of defects present in the carbon-based structures to impregnate them with transition metal atom [16-22] with the objective to boost their affinities to target CWAs. Although such a strategy allows the enhancement of the interactions between the adsorbent and the molecules we wish to capture [23-27], it might lead to competitive adsorption with other polar molecules present under specific operating conditions. A humidified environment is a major concern regarding the efficiency of activated carbons, typically in regards of diverse polar molecules including a series of volatile organic compounds [28-35]. While carbon-based materials are mostly hydrophobic [36] implying that water is not expected to interfere with the capture of the target molecules, the impregnation of carbons with transition metal atoms might lead to an enhancement of the hydrophilicity of the resulting materials [36-39]. Hence, the hydrophilic character of the impregnated carbons is potentially an obstacle to their efficient use for CWA capture. In the field of respiratory protection devices for civilian and military purposes [40], aging of activated carbons cartridges [41] or their uses under high relative humidity are two potential drawbacks that might alter the protection of the users. In this field, most of the theoretical studies on the adsorption performance of carbons in the presence of humidity have been limited to the application of macroscopic models to assess the lifetime of the corresponding cartridges [42-46]. While the microscopic exploration of CWA adsorption on metal oxides surfaces in the presence of water [47, 48] is well documented, this has never been achieved so far for any CWA/carbon systems.

To address this lack of microscopic insight, here we propose a computational exploration of the competitive adsorption of CWA and water on metal impregnated carbons. To that

purpose, periodic Density Functional Theory calculations (DFT) were performed to predict the impact of water on the interactions between three representative CWA molecules i.e., sarin, soman and mustard gas, and a graphene layer embedding one transition metal atom either Chromium (Cr) or Vanadium (V). Such a microscopic carbon model has been already successfully used to gain insight into the interactions between diverse toxic molecules and impregnated carbons [49-51]. Both pre-humidification and simultaneous competitive adsorption of water with CWAs were considered and the resulting preferential arrangements and associated energetics were assessed. As a further stage, a careful analysis of the electronic features of the corresponding H_2O/CWA/carbon systems was conducted to gain insight into the microscopic origin of the corresponding competitive adsorption phenomena on the carbon-substrates.

2. Computational details

The metal-embedded graphene models labelled metal@graphene were first built by substituting one carbon atom of a 5×5 graphene sheet ($12.30 \text{ Å} \times 12.30 \text{ Å}$) by a transition metal atom i.e. either Chromium or Vanadium. A length of 20 Å along the z-direction was considered to avoid interactions between their periodically replicated images. 1 molecule of each CWA, i.e., sarin, soman and mustard gas was further incorporated in these models using different starting configurations. DFT geometry optimizations were further performed using the PBE functional [52] and the DFT+D2 [53] dispersion correction as implemented in the Quantum Espresso package [54]. The D2 dispersion correction was demonstrated to accurately describe the interactions between polar molecules and impregnated carbons [55]. Ultrasoft Vanderbilt pseudopotentials [56] were used to describe ion cores of atom. An energy cut-off of 80 Ry was applied in combination with a convergence criteria on the energy of 1×10^{-5} Ry. A Gaussian smearing with $\sigma = 0.01$ was employed for the two transition metals. Monkhorst-Pack grids of k-points replicating the graphene sheet dimensions was considered.

To further explore the impact of water, two scenarios were considered mimicking either a pre-humidification condition or a simultaneous H_2O/CWA adsorption. In the first case, one water molecule was initially incorporated in the metal-embedded graphene models and then DFT-geometry optimized prior to introduce one CWA molecule. In the second scenario, both water and CWA molecules were simultaneously adsorbed and their geometries were further DFT-geometry optimized. In all these calculations, several starting configurations were considered corresponding to various positions of water and different orientations of the CWA molecules, i.e, parallel and perpendicular to the graphene sheet as well as with either F or O and S or Cl atoms pointing towards the metal sites for sarin/soman and mustard gas respectively, to ensure convergence towards minimum energy states.

The adsorption energies for the 3 CWAs were further calculated as follows:

(i) In the absence of water E_{ads} was obtained using equation 1:

$$E_{ads} = E_{Molecule/Metal@graphene} - (E_{Molecule} + E_{Metal@graphene}) \qquad (1)$$

where $E_{Molecule/Metal@graphene}$ is the energy of the DFT-optimized molecule/metal@graphene complex while $E_{molecule}$ and $E_{Metal@graphene}$ correspond to the single point energy of the single constituents, i.e. CWA and metal/graphene respectively.

(ii) in the presence of water, $E_{ads}^{H_2O}$ was obtained using equation 2:

$$E_{ads}^{H_2O} = E_{Molecule/H_2O - Metal@graphene} - (E_{Molecule} + E_{H_2O - Metal@graphene}) \quad (2)$$

where $E_{Molecule/H_2O - Metal@graphene}$ is the energy of the DFT-optimized molecule/H$_2$O - metal@graphene complex while $E_{molecule}$ and $E_{H_2O - Metal@graphene}$ are the single point energies of the single constituents, i.e. CWA and H$_2$O - metal@graphene complex respectively.

Such a definition of the adsorption energy for CWA allows the evaluation of the role of water on the strength of the CWA/substrate interactions.

3. Results and Discussion

Fig. 1 reports the DFT optimized structures for soman and mustard gas/metal@graphene models. We can observe in all cases an out-of-plane shift of the metal sites upon adsorption that become more exposed to CWAs (see **Tables S1-S2)**. Soman was found to interact preferentially with the metal center via its oxygen atom in a similar way than sarin [57]. Soman shows an equivalent adsorption behavior in the case of V@graphene (**Fig. 1 (a)**) and Cr@graphene (**Fig. 1 (b)**), with associated O(soman)-Metal interacting distance that only slightly varies from 2.06 to 2.00 Å respectively. The scenario differs for mustard gas which implies a preferential interaction between its central sulfur atom and the metal sites (**Fig. 1 (c)**) and **Fig. 1 (d)**). This observation was confirmed by considering different initial configurations where the chlorine atom of mustard gas was positioned in the vicinity of the metal sites (see **Tab. S3**). These calculations evidenced that the interacting S(mustard gas)-Metal distance is shorter for Chromium (2.34 Å) (**Fig. 1 (d)**) as compared to Vanadium (2.50Å) (**Fig. 1 (c)**).

The adsorption energies associated with the most stable DFT-optimized structures (**Fig. 1**) are reported in **Tab. 1**, while the corresponding data previously obtained for sarin are reminded for comparison [57]. One observes that the adsorption energies for soman and mustard gas are similar for both V@graphene and Cr@graphene, this behavior confirming our previous finding that V and Cr enable very similar strength of interactions for a given CWA molecule [57]. Furthermore, the adsorption energy sequence is as follows: E_{ads}(sarin) > E_{ads}(mustard gas) > E_{ads}(soman), the corresponding values varying in the range of 39.71 - 43.84 kcal.mol^{-1}, and 38.48 - 43.00 kcal.mol^{-1} for Cr@graphene and V@graphene respectively. This trend highlights that both metal-impregnated carbons show a slightly higher affinity for sarin vs the other two CWAs.

Fig. 2 reports the projected density of states (PDOS) for the soman/Cr@graphene and mustard gas/Cr@graphene complexes under dry conditions. Same analysis for the V-analogues can be found in **Fig. S1**. The total density of states is projected in such a way to represent the contributions of the orbitals of each interacting atoms, i.e. p- orbitals of P, F and O atoms for soman, p- orbitals of S and Cl atoms for mustard gas, s- and p- orbitals of C atoms for graphene as well as s-, p- and d- orbitals of the metal atom. One first notes the presence of a peak at the Fermi level which corresponds to a contribution of the p- orbitals of the carbon atom of the graphene sheet and the d- orbitals of Cr atom. This results from a hybridization phenomenon due to a shift in position of the metal out of the graphene plane. More specifically, in the case of soman/Cr@graphene complex, one can note that the peak corresponding to p- orbitals of the O atoms of soman is shifted of around -1eV, towards lowest energy compared to that of the isolated molecule. The peaks corresponding to p- orbitals of S and Cl of mustard gas adsorbed on Cr@graphene are shifted to a lesser extend towards lowest energy compared to the isolated state, leading to a small overlap of these orbitals of CWA with d- orbitals of Cr atom. Nonetheless, same trend is observed for both complexes at high energy. In particular, the peak situated initially around 1 eV, corresponding to d- orbitals of Cr atom, is shifted at higher energy when both CWAs are adsorbed. This evidences that, even by considering CWAs of different chemical nature, specifically organophosphorus and sulfur-based compounds, a similar hybridization is observed between the d- orbitals of chromium atom and the orbitals of the adsorbed molecules.

In order to further explore the electronic features of the CWA/Cr@graphene complexes, **Fig. 3** presents their charge density differences computed using a Bader charge analysis [58]. In both cases, a major accumulation of electron density is observed in the region situated between the Cr atom and the interacting atom of soman (**Fig. 3 (a)**) and mustard gas (**Fig. 3 (b)**) respectively. It can be observed that the expansion of this charge accumulation region is much more pronounced for mustard gas. This is attributed to the fact that in addition to the sulfur atom, the chlorine atom of the CWA also establishes side interactions with Cr atom while soman exclusively interacts through its oxygen atom.

As a further stage, we explored the impact of water on the adsorption of CWAs on metal@graphene. **Fig. 4** reports the DFT-optimized structures for all CWAs on Cr@graphene for the pre-humidification scenario. The analogue for V@graphene is represented in **Fig. S2**. One can observe that H_2O is strongly bounded to the metal sites in the presence of all CWAs with characteristic separating $O(H_2O)$-Cr distances of 2.03-2.05 Å. H_2O molecule establishes a strong hydrogen bond via its H atom with the oxygen atom of both soman and sarin (separating distances of 1.57-1.58 Å) while its two hydrogen atoms interact each with one chlorine atom of the mustard gas. Indeed, in this scenario, the interactions between CWA and the metal@graphene substrate are shielded by the water molecule that acts as a bridge between the two components.

We then explored the case of a simultaneous co-adsorption of water and CWAs. **Fig. 5** and **Fig S3** report the corresponding DFT-optimized structures for both H_2O on Cr and on V@graphene, respectively. **Table S4** indicates that the so-obtained configurations are significantly more energetically stable than those obtained for the pre-humidification scenario. Referring to soman molecule, a small elongation of the distance between the oxygen atom and the chromium atom is observed with respect to the dry state from 2.00 Å to 2.08 Å (**Fig. 5 (a)**) on Cr@graphene and from 2.06 Å to 2.13 Å (**Fig. S3a**) on V@graphene. Furthermore, the inclusion of water leads to a reduction of the adsorption energy for soman of -5.40 kcal.mol^{-1}, and -7.58 kcal.mol^{-1} in the cases of Cr@graphene and V@graphene, respectively (**Tab. 1**).

Regarding sarin, as compared to the dry states, the presence of water also leads to a slight elongation of the distance between the oxygen atom of the CWA and the metal site, i.e. from 2.00 Å [57] to 2.08 Å (**Fig. 5 (b)**) and from 2.06 Å [57] to 2.10 Å (**Fig. S3 (b)**) for Cr@graphene and V@graphene respectively. This translates into a decrease of the adsorption energy between sarin and the metal@graphene substrate for Cr (-8.91 kcal.mol^{-1}) and V (-6.80 kcal.mol^{-1}) once water is present as reported in Tab**. 1.** Finally in the case of gas mustard, the interacting distances between the sulfur atom and the metal atom vary from 2.34 Å to 2.51 Å (Cr@graphene – **Fig. 5 (c)**) and from 2.50 Å to 2.52 Å (V@graphene – **Fig. S3 (c)**) in the presence of water. In the case of Cr@graphene the significant elongation of the S-Cr distance is accompanied by a large reduction of the Cl-Cr distance from 3.28 Å to 2.72 Å, while the opposite is observed for V@graphene (2.69 Å to 3.16 Å). Nonetheless, as for soman and sarin, the presence of water leads to a reduction of the adsorption energies for mustard gas in the cases of Cr@graphene and V@graphene, however the decrease is of much lower magnitude, -1.37 kcal.mol^{-1} and -4.61 kcal.mol^{-1} respectively compared to the situation described above for sarin and soman (**Tab. 1**).

To summarize, **Tab. 1** evidences that the CWA/metal@graphene adsorption energy remains substantial even in the presence of water and this implies that the CWAs are expected to remain efficiently captured by the corresponding impregnated carbons under humidity. This is reflected by a decrease of maximum 20% of the adsorption energy, in the presence of water, for soman - sarin respectively in both metal@graphene. Interestingly, this conclusion is even more valid for mustard gas, its interaction with the impregnated carbons being much less affected by water as stated by the very low adsorption energy decrease (3.3%) in the case of Cr@graphene substrate. To understand the origin of this slightly different behavior, we further conducted a Density of states analysis (**Fig. 6**) on the soman/H_2O - Cr@graphene and mustard gas/H_2O - Cr@graphene complexes.

DOS of soman and mustard gas on H_2O - Cr@graphene plotted in **Fig. 6**, are projected in a similar way as in **Fig. 2**, to highlight the water-induced modifications of the electronic states, the same analysis for the V-analogue being reported in **Fig. S4**. By comparing **Fig. 2 (a)** and **Fig. 6 (a)**, one can note that for soman, similarly as under dry conditions, below the Fermi level, an overlap between p- orbitals of the oxygen atom of soman and d- orbitals of Cr is

reduced to a small contribution around -5 eV. Moreover, at higher energy (about 2.5 eV), a reduction of the overlap between d- orbitals of Cr and p- orbitals of O, P and F atoms of soman is observed. Since the interactions of soman on Cr@graphene take place mostly through its oxygen atom, these water-induced changes are associated with a weakening of the bonding established by the oxygen atom. On the other hand, by comparing **Fig. 2 (b)** and **Fig. 6 (b)** for mustard gas, one can note that the overlap between the p- orbitals of Cl and P (CWA) and the d- orbitals of Cr below the Fermi level is more pronounced and is present up to -3 eV. Furthermore, the intensity of d- orbitals of Cr increases above the Fermi level around 3 eV. This observation correlated with the geometry of the mustard gas molecule, where one Cl atom is in the vicinity of Cr (2.72 Å), is consistent with a rather small reduction of the adsorption energy for gas mustard on Cr@graphene in the presence of water. Regarding the V-analogue, the corresponding analysis reported **Fig. S4** shows that at high energy, above the Fermi level, the overlap observed between the p- orbitals of Cr and the p- orbitals of Cl and S atoms of the CWA (around 3.5 eV) is not anymore present. This lack of overlap contributes to a more pronounced reduction of the resulting adsorption energy in the case of V@graphene (-4.61 kcal.mol^{-1}) vs Cr@graphene (-1.37 kcal.mol^{-1}) upon water adsorption.

Fig. 7 and **Fig. 8** report the charge differences for each CWA (soman, sarin and mustard gas)/H$_2$O - Cr@graphene and V@graphene complexes respectively with an isovalue of $\pm 1.0 \times 10^{-3} e.\text{Å}^{-3}$. The comparison of **Fig. 7** with its analogue for the dry state (**Fig. 3**) reveals that the presence of water induces a deformation of the electronic density surrounding the interacting atom (oxygen for soman and sarin, sulfur for mustard gas) for the Cr@graphene complex. For each CWA, the depletion region on the metal is deformed towards the single water molecule leading to an elongation of the distance between the CWAs and the metal atom and therefore to a weakening of the interaction between CWAs and the substrate through their main interacting atom. Indeed, the interacting region between the H$_2$O – substrate with the CWAs is composed mostly by a depletion region of electronic density whereas accumulation phenomenon arises along the closest contact between the interacting atom of CWAs and the water oxygen atom. It can be seen that the electronic density deformation is made of the depletion regions on both top of the metal and at the vicinity of the water molecule that merged. This observation positions the water molecule as an extension of the metal@graphene substrate. The particular geometry of mustard gas molecule allows a side interaction between its chlorine atom and the metal atom which is less impacted by the presence of water as compared to the main interaction between metal and sulfur. While the only contact between soman and sarin on Cr@graphene is screened by the water molecule, the particularity of mustard gas geometry allows it to bypass this screening effect and to maintain a stabilizing contact resulting in a smaller adsorption energy reduction on Cr@graphene.

As expected from the variation of the adsorption energy observed for sarin between dry and simultaneous co-adsorption on Cr (-8.91 kcal.mol^{-1}) and V@graphene (-6.80 kcal.mol^{-1}), **Fig. 8** shows that similar electronic deformations are observed for both systems with the inclusion of simultaneous co-adsorbed water. The same observation about the electronic behavior can be made from **Fig. 7 (a)** and **Fig. 8 (a)** for soman even though the variation of adsorption energy is superior for V@graphene (-7.58 kcal.mol^{-1}) vs Cr@graphene (-5.40 kcal.mol^{-1}). Alternatively, the electronic charges differences comparison relative to mustard gas on Cr@graphene (**Fig. 7 (c)**) with V@graphene (**Fig. 8 (c)**) provides some highlights about the more pronounced reduction observed with V@graphene rather than Cr@graphene. The separating distance associated with the Cl-metal side interactions equal to 2.72 Å and 3.15 Å, for Cr and V@graphene complexes respectively, emphasizes the distinctive deformations of this specific depletion region observed for both systems. This distinct behavior is at the origin of the different adsorption energy variations reported for mustard gas/Cr@graphene and mustard gas/V@graphene between dry and wet conditions.

4. Summary

The adsorption of soman, sarin and gas mustard on Vanadium and Chromium embedded graphene models was computationally explored under dry and wet conditions. Our DFT calculations first demonstrated the highly attractive features of these impregnated carbons in terms of affinity with respect to the three considered CWAs. Both metal-impregnated carbons were predicted to show a slightly higher affinity for sarin vs the other two CWAs. As a further stage, we explored the impact of water on the physisorption of the three CWAs considering two scenarios, i.e. pre-humidification and simultaneous co-adsorption. The inclusion of water was shown to not dramatically alter the host/CWAs interactions, gas mustard being the less impacted molecule with an associated decrease of the adsorption energy by only 3.3% in Cr@graphene vs from 13 to 20% for sarin and soman. Indeed, the CWAs are expected to remain efficiently captured by the corresponding impregnated carbons under humidity. This microscopic investigation demonstrated the transition metal embedded@graphene systems to maintain a high level of performance for the capture of CWAs even in the presence of humidity, which corresponds to the most common operating conditions for protective gas masks.

References

[1] S. Chauhan, R. D'cruz, S. Faruqi, K. Singh, S. Varma, M. Singh, V. Karthik, Chemical warfare agents, Environmental Toxicology and Pharmacology, 26 (2008) 113-122.

[2] N.H. Johnson, J.C. Larsen, E. Meek, Historical perspective of chemical warfare agents, in: Handbook of Toxicology of Chemical Warfare Agents, Elsevier, 2009, pp. 7-16.

[3] A. Mangerich, C. Esser, Chemical warfare in the First World War: reflections 100 years later, Archives of Toxicology, 88 (2014) 1909-1911.

[4] D. Nelson, C. Crawford, Organophosphorus compounds; the past and the future, Clinical toxicology, 5 (1972) 223-230.

[5] L. Karalliedde, N. Senanayake, Organophosphorus insecticide poisoning, British journal of anaesthesia, 63 (1989) 736-750.

[6] F. Barnaby, Iran-Iraq War: the use of chemical weapons against the Kurds, Ambio, 17 (1988) 407-408.

[7] J. Dingeman, R. Jupa, Chemical warfare in the Iran–Iraq conflict, Strategy & Tactics, 113 (1987) 51-52.

[8] K. Yokoyama, A. Yamada, N. Mimura, Clinical profiles of patients with sarin poisoning after the Tokyo subway attack, The American journal of medicine, 100 (1996) 586.

[9] T. Okumura, N. Takasu, S. Ishimatsu, S. Miyanoki, A. Mitsuhashi, K. Kumada, K. Tanaka, S. Hinohara, Report on 640 victims of the Tokyo subway sarin attack, Annals of emergency medicine, 28 (1996) 129-135.

[10] K.-J. Kim, C.-S. Kang, Y.-J. You, M.-C. Chung, M.-W. Woo, W.-J. Jeong, N.-C. Park, H.-G. Ahn, Adsorption–desorption characteristics of VOCs over impregnated activated carbons, Catalysis Today, 111 (2006) 223-228.

[11] D. Kaplan, L. Shmueli, I. Nir, D. Waysbort, I. Columbus, Degradation of adsorbed sarin on activated carbons: a 31P-MAS-NMR study, CLEAN–Soil, Air, Water, 35 (2007) 172-177.

[12] S. Wang, H. Ang, M.O. Tade, Volatile organic compounds in indoor environment and photocatalytic oxidation: state of the art, Environment international, 33 (2007) 694-705.

[13] J. Dai, J. Yuan, P. Giannozzi, Gas adsorption on graphene doped with B, N, Al, and S: a theoretical study, Applied Physics Letters, 95 (2009) 232105.

[14] A. Junkaew, C. Rungnim, M. Kunaseth, R. Arróyave, V. Promarak, N. Kungwan, S. Namuangruk, Metal cluster-deposited graphene as an adsorptive material for m-xylene, New Journal of Chemistry, 39 (2015) 9650-9658.

[15] S. Wang, Z. Zhu, A. Coomes, F. Haghseresht, G. Lu, The physical and surface chemical characteristics of activated carbons and the adsorption of methylene blue from wastewater, Journal of Colloid and Interface Science, 284 (2005) 440-446.

[16] I.A. Pašti, A. Jovanović, A.S. Dobrota, S.V. Mentus, B. Johansson, N.V. Skorodumova, Atomic adsorption on graphene with a single vacancy: systematic DFT study through the periodic table of elements, Physical Chemistry Chemical Physics, 20 (2018) 858-865.

[17] S. Gupta, N. Dimakis, Computational predictions of electronic properties of graphene with defects, adsorbed transition metal-oxides and water using density functional theory, Applied Surface Science, 467 (2019) 760-772.

[18] L. Hu, X. Hu, X. Wu, C. Du, Y. Dai, J. Deng, Density functional calculation of transition metal adatom adsorption on graphene, Physica B: Condensed Matter, 405 (2010) 3337-3341.

[19] S. Jungsuttiwong, Y. Wongnongwa, S. Namuangruk, N. Kungwan, V. Promarak, M. Kunaseth, Density functional theory study of elemental mercury adsorption on boron doped

graphene surface decorated by transition metals, Applied Surface Science, 362 (2016) 140-145.

[20] H. Wang, Q. Wang, Y. Cheng, K. Li, Y. Yao, Q. Zhang, C. Dong, P. Wang, U. Schwingenschlögl, W. Yang, Doping monolayer graphene with single atom substitutions, Nano letters, 12 (2011) 141-144.

[21] E.J. Santos, A. Ayuela, D. Sánchez-Portal, First-principles study of substitutional metal impurities in graphene: structural, electronic and magnetic properties, New Journal of Physics, 12 (2010) 053012.

[22] C.-Y. Lu, M.-Y. Wey, Simultaneous removal of VOC and NO by activated carbon impregnated with transition metal catalysts in combustion flue gas, Fuel Processing Technology, 88 (2007) 557-567.

[23] M. Kunaseth, T. Mudchimo, S. Namuangruk, N. Kungwan, V. Promarak, S. Jungsuttiwong, A DFT study of arsine adsorption on palladium doped graphene: effects of palladium cluster size, Applied Surface Science, 367 (2016) 552-558.

[24] A. Krasheninnikov, P. Lehtinen, A.S. Foster, P. Pyykkö, R.M. Nieminen, Embedding transition-metal atoms in graphene: structure, bonding, and magnetism, Physical review letters, 102 (2009) 126807.

[25] L. Ma, J.-M. Zhang, K.-W. Xu, V. Ji, Hydrogen adsorption and storage on palladium-decorated graphene with boron dopants and vacancy defects: a first-principles study, Physica E: Low-dimensional Systems and Nanostructures, 66 (2015) 40-47.

[26] Y.-H. Lu, M. Zhou, C. Zhang, Y.-P. Feng, Metal-embedded graphene: a possible catalyst with high activity, The Journal of Physical Chemistry C, 113 (2009) 20156-20160.

[27] C. Ramos-Castillo, J. Reveles, R. Zope, R. De Coss, Palladium clusters supported on graphene monovacancies for hydrogen storage, The Journal of Physical Chemistry C, 119 (2015) 8402-8409.

[28] A. Slasli, M. Jorge, F. Stoeckli, N. Seaton, Water adsorption by activated carbons in relation to their microporous structure, Carbon, 41 (2003) 479-486.

[29] C. McCallum, T. Bandosz, S. McGrother, E. Müller, K. Gubbins, A molecular model for adsorption of water on activated carbon: comparison of simulation and experiment, Langmuir, 15 (1999) 533-544.

[30] C.-C. Huang, C.-H. Chen, S.-M. Chu, Effect of moisture on H2S adsorption by copper impregnated activated carbon, Journal of hazardous materials, 136 (2006) 866-873.

[31] L. Jing, L. Zhong, L. Bing, X. Qibin, X. Hongxia, Effect of relative humidity on adsorption of formaldehyde on modified activated carbons, Chinese Journal of Chemical Engineering, 16 (2008) 871-875.

[32] R. Sitthikhankaew, D. Chadwick, S. Assabumrungrat, N. Laosiripojana, Effects of humidity, O2, and CO2 on H2S adsorption onto upgraded and KOH impregnated activated carbons, Fuel processing technology, 124 (2014) 249-257.

[33] Y.-C. Chiang, Y.-J. Chen, C.-Y. Wu, Effect of relative humidity on adsorption breakthrough of CO2 on activated carbon fibers, Materials, 10 (2017) 1296.

[34] S. Qi, K.J. Hay, M.P. Cal, Predicting humidity effect on adsorption capacity of activated carbon for water-immiscible organic vapors, Advances in Environmental Research, 4 (2000) 357-362.

[35] J.K. Brennan, T.J. Bandosz, K.T. Thomson, K.E. Gubbins, Water in porous carbons, Colloids and surfaces A: Physicochemical and engineering aspects, 187 (2001) 539-568.

[36] E.A. Müller, K.E. Gubbins, Molecular simulation study of hydrophilic and hydrophobic behavior of activated carbon surfaces, Carbon, 36 (1998) 1433-1438.

[37] A.J. Fletcher, Y. Yüzak, K.M. Thomas, Adsorption and desorption kinetics for hydrophilic and hydrophobic vapors on activated carbon, Carbon, 44 (2006) 989-1004.

[38] F. Ahnert, H.A. Arafat, N.G. Pinto, A study of the influence of hydrophobicity of activated carbon on the adsorption equilibrium of aromatics in non-aqueous media, Adsorption, 9 (2003) 311-319.

[39] Y. Xiang, L. Kong, P. Xie, T. Xu, J. Wang, X. Li, Carbon nanotubes and activated carbons supported catalysts for phenol in situ hydrogenation: Hydrophobic/hydrophilic effect, Industrial & engineering chemistry research, 53 (2014) 2197-2203.

[40] P. Sharma, V. Singh, N. Tripathi, M. Sathe, V. Verma, S.P. Sharma, L. Tomar, A. Chaturvedi, S. Yadav, V.B. Thakare, Chemical Protection Studies of Activated Carbon Spheres based Permeable Protective Clothing Against Sulfur Mustard, a Chemical Warfare Agent, Defence Science Journal, 69 (2019).

[41] T. Amitay-Rosen, A. Leibman, I. Nir, A. Zaltsman, D. Kaplan, The Effects of Aging on the Dynamic Adsorption of Hazardous Organic Vapors on Impregnated Activated Carbon, Journal of occupational and environmental hygiene, 12 (2015) 130-137.

[42] G. Wood, P. Lodewyckx, Correlations for High Humidity Corrections of Rate Coefficients for Adsorption of Organic Vapors and Gases on Activated Carbons in Air-Purifying Respirator Cartridges, JOURNAL-INTERNATIONAL SOCIETY FOR RESPIRATORY PROTECTION, 19 (2002) 58-64.

[43] G.O. Wood, Affinity coefficients of the Polanyi/Dubinin adsorption isotherm equations: A review with compilations and correlations, Carbon, 39 (2001) 343-356.

[44] P. Lodewyckx, E. Vansant, The influence of humidity on the overall mass transfer coefficient of the Wheeler-Jonas equation, AIHAJ-American Industrial Hygiene Association, 61 (2000) 461-468.

[45] T. Hall, P. BREYSSE, M. Corn, L. Jonas, Effects of adsorbed water vapor on the adsorption rate constant and the kinetic adsorption capacity of the Wheeler kinetic model, American Industrial Hygiene Association Journal, 49 (1988) 461-465.

[46] A.J. Fletcher, Y. Uygur, K.M. Thomas, Role of surface functional groups in the adsorption kinetics of water vapor on microporous activated carbons, The Journal of Physical Chemistry C, 111 (2007) 8349-8359.

[47] Y.C. Quintero, R. Nagarajan, Molecular and dissociative adsorption of DMMP, Sarin and Soman on dry and wet TiO2 (110) using density functional theory, Surface Science, 675 (2018) 26-35.

[48] G.W. Wagner, G.W. Peterson, J.J. Mahle, Effect of adsorbed water and surface hydroxyls on the hydrolysis of VX, GD, and HD on titania materials: the development of self-decontaminating paints, Industrial & engineering chemistry research, 51 (2012) 3598-3603.

[49] H.-K. Dong, Y.-P. Wang, L.B. Shi, First principles study of HCN adsorption on graphene doped with 5d transition metal, Surface Review and Letters, 23 (2016) 1550095.

[50] M. Kunaseth, P. Poldorn, A. Junkeaw, J. Meeprasert, C. Rungnim, S. Namuangruk, N. Kungwan, C. Inntam, S. Jungsuttiwong, A DFT study of volatile organic compounds adsorption on transition metal deposited graphene, Applied Surface Science, 396 (2017) 1712-1718.

[51] N.K. Jaiswal, G. Kovačević, Sarin chemisorbent based on cobalt-doped graphene, Applied Surface Science, 480 (2019) 759-764.

[52] J.P. Perdew, Y. Wang, Accurate and simple analytic representation of the electron-gas correlation energy, Physical Review B, 45 (1992) 13244.

[53] S. Grimme, Semiempirical GGA-type density functional constructed with a long-range dispersion correction, Journal of computational chemistry, 27 (2006) 1787-1799.

[54] P. Giannozzi, S. Baroni, N. Bonini, M. Calandra, R. Car, C. Cavazzoni, D. Ceresoli, G.L. Chiarotti, M. Cococcioni, I. Dabo, QUANTUM ESPRESSO: a modular and open-source software project for quantum simulations of materials, Journal of physics: Condensed matter, 21 (2009) 395502.
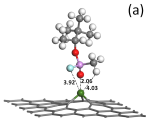
[55] Jogender, Mandeep, B. Badhani, R. Kakkar, Adsorption of methyl isocyanate on M-4 (M= Fe, Ni, and Cu) cluster-decorated graphene and vacancy graphene: a DFT-D2 study, STRUCTURAL CHEMISTRY, (2020).

[56] D. Vanderbilt, Soft self-consistent pseudopotentials in a generalized eigenvalue formalism, Physical review B, 41 (1990) 7892.

[57] J. Claudot, E. Soubeyrand-Lenoir, G. Maurin, Computational exploration of Sarin and simulants adsorption on a series of transition metal embedded graphene, Applied Surface Science, (2020) 148047.

[58] W. Tang, E. Sanville, G. Henkelman, A grid-based Bader analysis algorithm without lattice bias, Journal of Physics: Condensed Matter, 21 (2009) 084204.

Figure captions

Figure 1   Most stable DFT-optimized configurations of soman on (a) V@Graphene and (b) Cr@graphene as well as of mustard gas on (c) V@graphene (d) Cr@graphene under dry conditions.

Figure 2   Comparison of PDOS for the (a) Soman/Cr@graphene and (b) Mustard gas/Cr@graphene complexes under dry conditions. For each system panel I, panel II and panel III present PDOS of the isolated CWA, isolated metal@graphene and resulting complexes. O_p (soman), F_p (soman), P_p (soman), Cl_p (mustard gas), S_p (mustard gas), C_s (CWA), C_p (CWA), C_s (graphene), C_s (graphene), total DOS of molecule, s-, p-, and d- states of metal are represented in orange, light green, violet, dark green, cyan, dashed blue, dashed red, blue, red, black, bold blue, bold red, bold black, respectively.

Figure 3   Charge differences for (a) Soman/Cr@graphene and (b) Mustard gas/Cr@graphene presented with isovalue of $\pm 1.0 \times 10^{-3} e . \text{Å}^{-3}$. Blue and red colors represent, respectively, the charge accumulation and depletion regions.

Figure 4   Most stable DFT-optimized configurations considering the pre-humidified scenario with one water molecule involved for (a) Soman/Cr@Graphene, (b) Sarin/Cr@graphene and (c) Mustard gas/Cr@graphene

Figure 5   Most stable DFT-optimized configurations considering a simultaneous co-adsorption of water molecule and CWA for(a) Soman/H_2O - Cr@graphene, (b) Sarin/H_2O - Cr@graphene and (c) Mustard gas/H_2O - Cr@graphene.

Figure 6   PDOS for the (a) Soman/H_2O - Cr@graphene and (b) Mustard gas/H_2O - Cr@graphene complexes in the case of the simultaneous co-adsorption scenario. For comparison, PDOS for the isolated CWA molecules and H_2O - Cr@graphene complexes are also reported. O_p (soman), F_p (soman), P_p (soman), Cl_p (mustard gas), S_p (mustard gas), C_s (CWA), C_p (CWA), C_s (graphene), C_s (graphene), total DOS of molecule, s-, p-, and d- states of metal are represented in orange, light green, violet, dark green, cyan, dashed blue, dashed red, blue, red, black, bold blue, bold red, bold black, respectively.

Figure 7   Charge differences considering the simultaneous co-adsorption scenario for (a) Soman/H_2O - Cr@graphene (b) Sarin/H_2O - Cr@graphene and (c) Mustard gas/H_2O - Cr@graphene complexes presented with isovalue of $\pm 1.0 \times 10^{-3} e . \text{Å}^{-3}$. Blue and red colors represent the charge accumulation and depletion regions respectively.
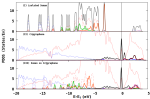
Figure 8   Charge differences considering the simultaneous co-adsorption scenario for (a) Sarin/H_2O - V@graphene (b) Soman/H_2O - V@graphene and (c) Mustard gas/H_2O - V@graphene complexes presented with isovalue of $\pm 1.0 \times 10^{-3} e.\text{Å}^{-3}$. Blue and red colors represent the charge accumulation and depletion regions respectively.
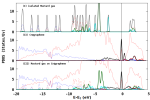
Table captions

Table 1   CWA dependence of the DFT calculated CWA adsorption energies (in kcal.mol^{-1}) for both V/Cr@graphene in the absence and in the presence of water. For comparison the CWA adsorption energies are also reported for the graphene without transition metal atom and without water.
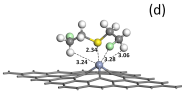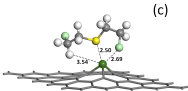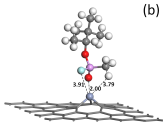
(a)

(b)

(c)

(d)

(a) Xenon on Cryographene

(b) Mustard gas on Cryographene

(a)   (b)

(a)

(b)

(c)

(a)
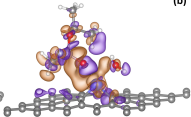
(b)

(c)

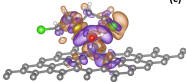(a) Sarpon in Water — Crigraphene
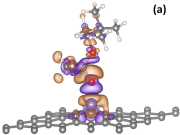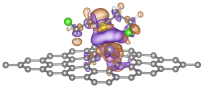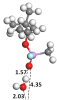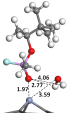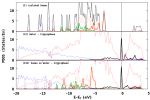
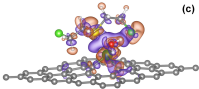(b) Mustard gas in Water — Crigraphene
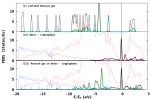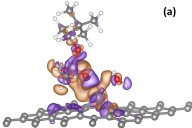
(a)   (b)

(c)

(a)
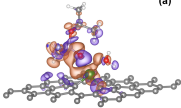
(b)
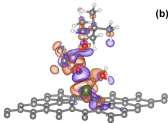
(c)

Table 1

	Cr@graphene		V@graphene		Pristine graphene
	No water	Water	No water	Water	
Soman	-39.71	-34.31	-38.48	-30.90	-1.79
Sarin	-43.84	-34.93	-43.00	-36.20	-1.84
Mustard gas	-40.91	-39.54	-41.60	-36.96	-2.10

Soman   Mustard gas   Sarin